Decision Tree Fusion and Improved Fundus Image Classification Algorithm

Xiaofang Wang[1(✉)] , Yanhua Qiu[2], Xin Chen[2], Jialing Wu[2],
Qianying Zou[1] , and Nan Mu[3]

[1] Geely University of China, Chengdu 641423, Sichuan, China
`939549393@qq.com`
[2] Chengdu College of University of Electronic Science and Technology of China,
Chengdu 611731, Sichuan, China
[3] Sichuan Normal University, Chengdu 610066, Sichuan, China

Abstract. In order to improve the effect of glaucoma fundus image classification, a new algorithm based on decision tree and UNet++ was proposed. Firstly, the image is divided into three channels of RGB, and the extracted green channel image is enhanced with the Butterworth parameter function of the fusion power function. Then the improved UNet++ network model is used to extract the texture features of the fundus image, and the residual module is used to enhance the texture features. The results of the experiment show that the average accuracy, the average specificity and the average sensitivity of the improved algorithm increase by 9.2%, 6.4% and 6.5% respectively. The improved algorithm is effective in glaucoma fundus image classification.

Keywords: Image classification · Butterworth parameter function · Improved UNet++ · Residual attention mechanism · Decision tree

1 Introduction

Glaucoma, as the second most common eye disorders in the world, is a group of eye conditions that damage the optic nerve [1]. It is the focus of fundus image separation detection research [2], and has attracted experts' attention.

Among them, He Xiaoyun et al. [3] put forward an improved UNet network model, which integrates residual block, cascade cavity convolution and embedded attention mechanism into UNet model to segment retinal vessels. Sabri Deari et al. [4] proposed a model of retinal vascular segmentation network based on migration learning strategy. The model was processed by pixel transformation and reflection transformation to enhance the data set. After processing, the retinal features were trained using the U-Net model to achieve retinal vascular segmentation; Yuan Zhou et al. [5] put forward the model of fusion attention mechanism and UNet++ network, based on UNet++ model, to achieve image feature extraction, and at the same time the attention mechanism is integrated

into convolution unit to achieve feature enhancement, and then complete end-to-end detection of image; Ali Serener [6] and others proposed an image classification algorithm based on a single CNN convolution neural network model. This method can realize glaucoma image classification by creating multiple fusion of CNN. Guo Pan et al. [7] proposed a glaucoma image detection method based on MobileNet v2 and VGG classification network. The method used MobileNet v2 segmentation model to segment and locate the VGG image. Gupta et al. [8] proposed a method for detecting retinal vessels in random forest classification. The method could segment retinal images and extract the texture and gray features of the blocks, and then classify the retinal images. Ke Shiyuan et al. [9] used Support Vector Machine and Logistic Regression Integrated Multi-View Learning to predict glaucoma; DAS et al. [10] proposed a method for glaucoma detection based on CDR and ISNT rules. The method used region-growing method and watershed transform to segment OC and OD, and then realized glaucoma image classification. Narmatha Venugopal et al. [11] put forward a method of glaucoma image classification based on PH-CNN model, which uses DWT and PCA fusion method to extract features, and then uses PH-CNN model to classify glaucoma image automatically.

Although these algorithms can screen and judge glaucoma fundus lesions, but the accuracy of glaucoma fundus lesions detection is low, and the classification is not good. Considering these problems, this paper proposes an improved UNet++ algorithm for glaucoma image classification and detection. Firstly, the Butterworth parameter function is used to enhance the color, texture and contrast of the fundus image, and then the UNet++ network based on residual thought and mixed field of attention is used to extract the feature.

2   Algorithmic Implementation

In order to solve the problem of low contrast in glaucoma image classification, an improved UNet++ algorithm based on decision tree fusion is proposed. The whole algorithm is divided into three stages: preprocessing, feature extraction and image classification. The architecture is shown in Fig. 1.

Figure 1 shows that in the preprocessing stage, the green component image is extracted, and then the texture information and contrast of the glaucoma fundus image are enhanced by power function Butterworth parameter function; In the feature extraction stage, UNet++ network based on residual error module and attention mechanism is used; Decision tree C4.5 is used to classify the fundus images, and the results of glaucoma detection are obtained.

2.1   Preprocessing

Aiming at the problems of low contrast and poor detail information of the image, the improved Butterworth parameter function with power function fusion is used to preprocess the fundus image. The processing process is to first separate the RGB image, extract the green component image (as shown in Fig. 2), and then
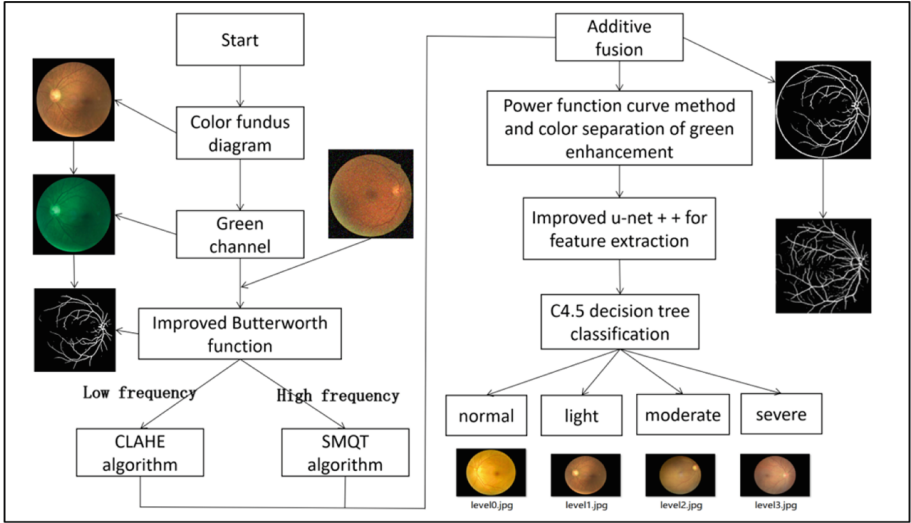
Fig. 1. Overall algorithm architecture diagram

use the improved Butterworth parameter function [12] to carry out frequency division processing to obtain high frequency information and low frequency information. The calculation is as shown in formula 1 and formula 2.

$$P_h = (R_h - R_l) / \left(1 + \frac{aD_0}{D(x,y)}\right) 2n + R_l \tag{1}$$

$$P_l = 1 - \left[(R_h - R_l) / \left(1 + \frac{aD_0}{D(x,y)}\right) 2n + R_l\right] \tag{2}$$

where R_h and R_l denote the high-frequency gain coefficient of the glaucoma fundus image and the low-frequency gain coefficient of the glaucoma fundus image. While $R_h > 1$, Represents high-frequency information that enhances fundus images.While $R_l < 1$, it is denotes reduced ocular fundus low-frequency information. a indicates the sharpening coefficient, D_0 indicates the cut-off frequency, n indicates the order of the filter, $D(x,y)$ indicates the distance between the frequency (x,y) and the filtering (x_0, y_0) center, and the Euclidean distance formula is adopted for calculation, as shown in formula 3.

$$D(x,y) = \sqrt[2]{(x - x_0)^2 + (y - y_0)^2} \tag{3}$$

After frequency division processing, high and low frequency information and low frequency information are obtained. In order to transform the information of high and low frequency into the image of high and low frequency for enhancement processing, inverse Fourier transform is used to transform the information of frequency domain into the image of spatial domain, as shown in formula 4.

$$F(t) = \frac{1}{2\pi} \int_{-\infty}^{+\infty} \mathrm{F(w)} e^{i\omega t} dw \tag{4}$$

where $F(t)$ represents a function of the time domain, $F(w)$ represents a function of frequency, and $F(t)$ is an imaginary function of F(w). After processing, high frequency image $F_h(x, y)$ and low frequency image $F_l(x, y)$ are obtained.

In order to enhance the local contrast and improve the texture details of the image, the SMQT algorithm [12] is used to extend the gray level region of the image to achieve nonlinear stretching of the gray level of the image to enhance the pixels. The SMQT function uses binary tree to deal with the pixels of the image, and overlaps the outputs of each layer linearly to get the locally enhanced high frequency image, as shown in formula 5.

$$F_h'(m) = \left\{ m \mid V(m) = \sum_{l=1}^{L} \sum_{n=1}^{2^{l-1}} V(u(l,n)) 2^{L-l}, \forall \in M, \forall u(l,n) \in \forall u(l,n) \right\} \tag{5}$$

where m represents a pixel in image $D(m)$, $F_h'(m)$ is the output of SMQT, $v(m)$ is the gray value of the pixel, $U(m)$ is the quantization of the gray value, L represents number of layers in the binary tree, and n is the MQN output number with the number of layers of l.

In order to reduce the influence of color component on image detection, the low-frequency image is converted into Lab space [13], and the L-channel is processed by the method of histogram equalization. The processing principle is to divide the image into several blocks, classify each block, and interpolate each pixel with histogram equalization method to get the F_l' of the processed gray image. The processed high-frequency image and low-frequency image are fused to get the enhanced fundus image. The processing is shown in formula 6.

$$G(x, y) = aF_h'(x, y) + bF_l'(x, y) \tag{6}$$

where a and b denote the weighted constant respectively, and $G(x, y)$ represent the enhanced eye ground green component.

In order to reduce the influence of external factors and ensure the integrity of fundus image structure, the power function curve method [14] is used to reduce noise. The power function adjusts the image contrast mode by parameters and adjusts by image mapping relation. The calculation is shown in formula 7.

$$G' = ax^t + bx^{(t-1)} + \ldots\ldots + cx + d \tag{7}$$

where t is a power, it is a controllable parameter after the processing of enhanced image preprocessing.

2.2   Feature Extraction

UNet++ Networkm

(a) DogLeg Method   (b) Steepest Descent Method
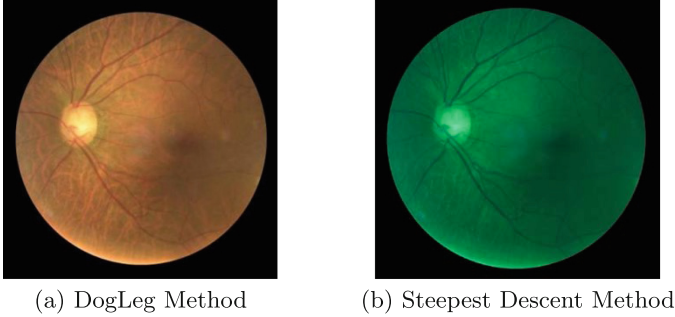
Fig. 2. Comparison result diagram

In order to extract texture and detail information of fundus image effectively and improve the effect of image feature extraction, an improved UNet++ network model is proposed. In order to avoid the overfitting problem in the training process, the residual error idea is introduced into the model based on the UNet++ network. In addition, in order to improve the performance of the network feature extraction, the mixed domain attention mechanism is added to the residual module to enhance the texture feature. Its network architecture is shown in Fig. 3. As can be seen from the diagram above, the UNet++ network [15] consists of an encoder and a decoder, $x^{(i,j)}$ represents the output of the node $x^{(i,j)}$, where i represents the number of layers, j represents the j convolution layer of the current layer, black represents the original UNet, green and blue represent the dense convolution blocks on the jump path, and red represents depth oversight. The hopping path is used to change the connectivity of the encoder and decoder subnetworks. In UNet, the decoder receives the encoder's feature map directly, whereas in UNet++ there is a dense convolution block, and all convolution layers on the jump path use cores of size 3 by 3. Deep supervision enables the UNet++ model to run in both accurate and fast mode, averaging the output of all split branches. Quick mode is used to split the graph.Finally, only one branch is selected, and the results are used to determine the model pruning degree and speed gain.

Residual Module and Attention Mechanism

To solve the problem of gradient disappearance, the residual module [16] is introduced between the sampling and down sampling convolution layers on the UNet++ network, and a mixed domain attention mechanism [17] is added before each residual convolution module to obtain more local and global texture information. The architecture of the residual module is improved as shown in Fig. 4.
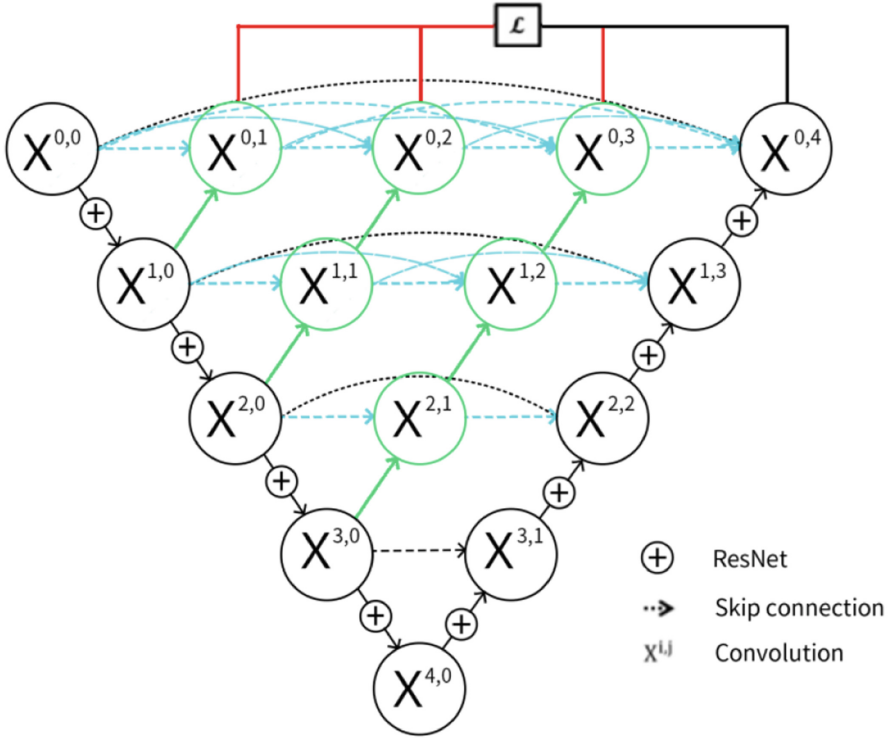
Fig. 3. Improved UNet++ model diagram

The principle of the residual module is to add the input feature graph and the feature extraction module to get the feature information, so that the network can contain the feature information of the input feature graph when propagating forward, and effectively solve the degradation problem of network model onvolution processing. The calculation is shown in Eq. 8.

$$H(x) = F(x) + x \tag{8}$$

where x represents the input network, $F(x)$ the feature extraction module, and $H(x)$ the output of the feature extraction of the eyeground image. In order to obtain specific feature texture information, the mixed domain attention mechanism is introduced into the residual error network. The network model in Fig. 5.

From Fig. 5, the input fundus feature map represents fed into the channel attention mechanism to perceive the global texture information, and the extracted information is fused with the original image to obtain the global feature processing results, as shown in formula 9.

$$CBAM\left(F_i\right) = SAM\left(CAM\left(F_i\right)\right) \times F_i \times \left(CAM\left(F_i\right) \times F_i\right) \tag{9}$$
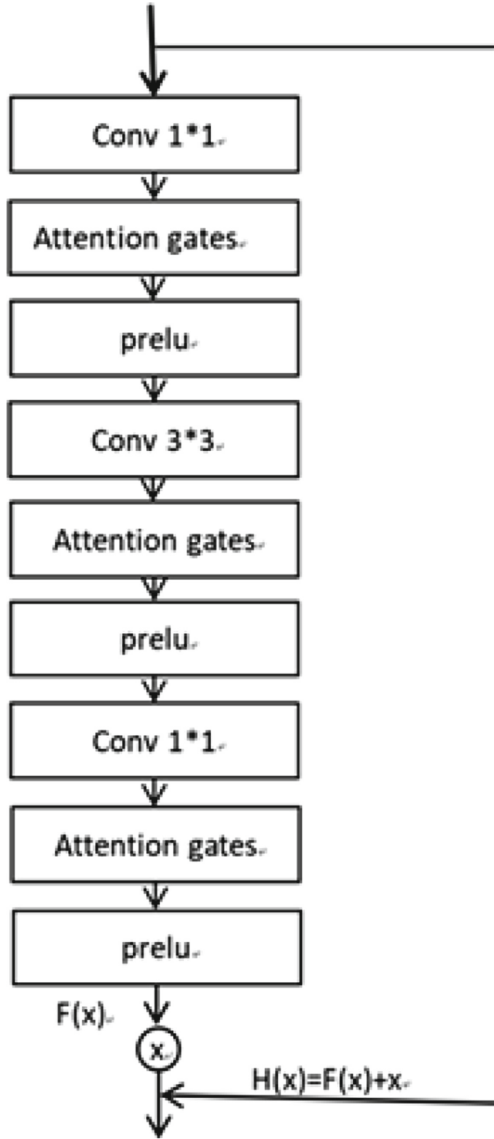
Fig. 4. Improved residual module structure diagram

where $CBAM(F_i)$ denotes the result of mixed domain attention mechanism, F_i denotes input fundus graph, $CAM(F_i)$ denote channel attention mechanism, SAM denote spatial attention mechanism, and $\times$ denotes matrix convolution.

The maximum pooling and the average pooling are then forwarded to a shared hidden layer MLP network. The dimensions of the two channel pooling maps are set to C $\times$ 1 $\times$ 1, and the result of the average pooling is processed by
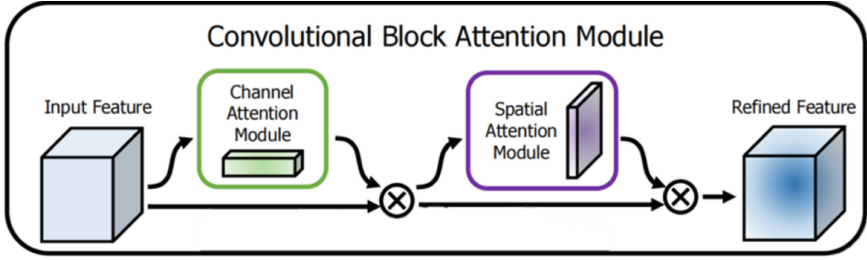
Fig. 5. Mixed domain attention mechanism

the sigmoid function. Finally, the result of the channel pooling is added to the result of the channel pooling mechanism as shown in formula 10.

$$CAM\left(F_i\right) = sigmod\left(MLP\left(AvgPool\left(F_i\right)\right) + MLP\left(MaxPool\left(F_i\right)\right)\right) \quad (10)$$

where sigmod is the activation function, the $AvgPool$ is the average pooling process, the $MaxPool$ is the maximum pooling process, and the MLP is the MLP neural network, that is, the multilayer perceptual process, with the number of neurons in the hidden layer set to C/r and the r as a hyperparameter.

The spatial attention mechanism is pooled along the channel axis by average and maximum pooling, and then the two characteristic graphs are spliced together for convolution operation. Finally, the processing result of spatial attention mechanism is obtained by sigmoid activation, and the calculation is shown in formula 10.

$$SAM\left(CAM\left(F_i\right)\right) = sigmod\left(conv\left(\left[AvgPool\left(M_c\right) + MaxPool\left(M_c\right)\right]\right)\right) \quad (11)$$

where SAM is the operation of spatial attention mechanism, and convolution operation is represented by $conv$.

Loss Function and Activation Function

To measure the classification error of the model, the improved UNet++ network uses the cross-entropy cost function as the loss function, and its calculation is shown in Formula 12.

$$C = -\frac{1}{n}\sum_x [y\ln a + (1-y)\ln(1-a)] \quad (12)$$

where y is the expected output of the glaucoma model, a represents the actual output of texture information, x represents sample data, and n represents the total sample size.

In order to optimize the network parameters, the stochastic gradient descent function is used as the optimization function. The principle is to select a part

of dataset from the training dataset by random processing. Keep updating, get the final result, its parameter updating formula is shown in formula 13.

$$\theta_j = \theta_j \vartheta * \frac{\partial JS(\theta_j)}{\partial \theta_j} \tag{13}$$

where S is the total number of training samples, and j represents the selected value of the samples, with a value of $\in [0, S]$.

The residual module is processed using PReLU [18] activation functions to reduce dependency on manual adjustments and reduce empiricism, as shown in Formula 14.

$$f(y_i) = \begin{cases} y_i, & \text{if } y_i \geq 0 \\ a_i y_i, & \text{if } y_i < 0 \end{cases} \tag{14}$$

where i is different channels, for residual processing, each channel has different parameters PReLU function. a_i represents the initialization value, and 0.25 is the best.

The sigmoid function in the attention mechanism is an S-shaped saturation function, calculated as Formula 15.

$$sigmod(y_i) = \frac{1}{1 + \exp(-y_i)} \tag{15}$$

2.3 Fundus Image Classification

To improve the classification effect of glaucoma fundus image and reduce the model training and detection practice, the multi-classification of glaucoma fundus lesions using c4.5 decision tree was studied [19].

The Decision Tree C4.5 algorithm is used to find split attributes from all texture information extracted from features, generate texture information and no texture information, continuously segment the nodes with texture information, and then classify glaucoma fundus lesions into normal, mild, moderate and severe glaucoma.

Decision tree C4.5 algorithm implementation is divided into two stages: initial decision tree generation and decision tree pruning. The algorithm flow is as follows:

input: Training set decision table: training set $DK = (d_1, k_1), (d_2, k_2), ...,$ (d_n, k_n) and set of attributes $AK = a_1, a_2, a_3, a_4$

output: Decision tree with Node as root node

1. function Build_DT(D,A) constructive function
2. generate node B
3. if samples is DK belong to the same category CK then
4. mark node as class CK leaf node; return
5. end if
6. if $AK = \emptyset$, samples in DK have the same value on AK then
7. mark B as a leaf node of the class with the most samples in DK return

8. end if
9. select the best attribute from AK, be $a_* = \arg\max_{a \in A} q_A^x GR(DK, a)$, attributes with the highest rate of gain
10. for a_* to every attribute value of a_*^v do
11. generate a branch for Node; make DK^v a subset of samples in DK that have a_* value of a_*^v
12. if DK^v is Null then
13. mark the branch node as the leaf node of the class with the most samples in DK
14. else
15. use Build_DT($DK^v, AK\ a_*$) as a branch node
16. end if
17. end for
18. end function

After the decision tree classification, the fundus image of glaucoma was detected to be normal, mild, moderate or severe.

3   Experimental Analysis

3.1   Experimental Environment

Data sets provided by Paddle Paddle were used and 480 glaucoma datasets were selected for training. Normal glaucoma, mild glaucoma, moderate glaucoma and severe glaucoma accounted for 120 each, as shown in Fig. 6.
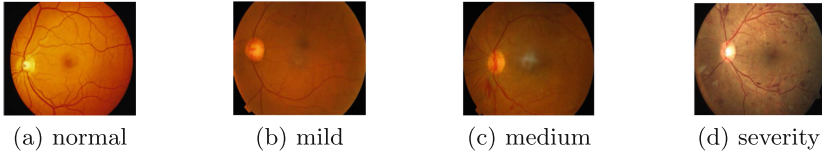

(a) normal   (b) mild   (c) medium   (d) severity

Fig. 6. Sample data set diagram

The study used Inteli7-7800 CPU, NVIDIA Ge Force GTX 1080i graphics card, Paddle Paddle 2G GPU, deep learning frameworks Keras, OpenCV and Tensorflow. Because the UNet++ network input layer requires 1024×1024 pixels, the Python pillow library is used to manipulate the crop to set a fixed clipping region to crop all images to 1024×1024 and train at a 7:3 scale.

3.2   Experimental Design and Analysis

Accuracy Acc, specificity S_p and sensitivity S_n were used to evaluate the classification of glaucoma fundus lesions, as shown in Formula 16, 17 and 18.

$$Acc = \frac{M + N}{M + N + L + P} \tag{16}$$

$$S_p = \frac{N}{N + P} \tag{17}$$

$$S_n = \frac{P}{P + L} \tag{18}$$

where M is the number of normal fundus maps, N is the number of glaucoma maps, L is the number of normal fundus maps, P is the number of glaucoma maps, and N and P represent the total number of glaucoma maps.

To obtain the global optimal effect of the loss function, the optimal learning rate of 0.001 is selected by adjusting the network weight super-parameters. The accuracy of different iterative experiments is analyzed during the model training, and the results in Fig. 7.
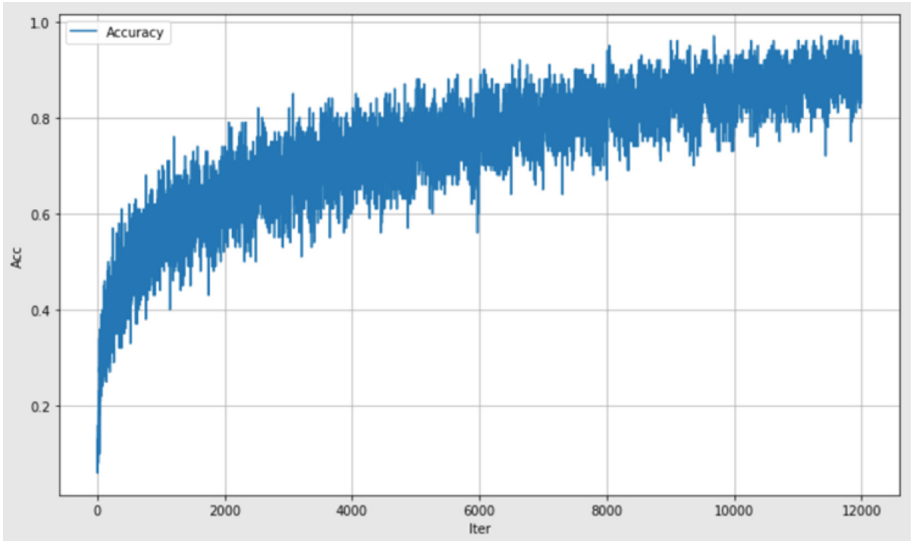

Fig. 7. Result chart of model average accuracy under different iterations

The results show that the average classification accuracy is the best when the learning rate is 0.001, and the average classification accuracy is 94.46%.

Analysis of Different Network Performance

In order to verify the effect of different algorithms on glaucoma fundus image classification under the same experimental environment, the accuracy, specificity and sensitivity of CNN, He [3], Sabri [4], Ali [6] and the algorithm presented in this paper are analyzed. The results are shown in Table 1.

Table 1. Performance analysis of different network models

Network	Acc	Sp	Sn
Classical CNN	78.86	79.12	81.32
He	88.03	89.25	93.78
Sabri	88.85	87.87	93.01
Ali	90.26	88.52	92.15
Proposed method	94.46	91.74	95.89

In Table 1, the average accuracy, the average specificity and the average sensitivity of glaucoma detection are all classical CNN algorithm. The best result is 94.46%, 91.74% and 95.89%. Compared with the traditional network model, the average accuracy, the average specificity and the average sensitivity are improved by 9.2%, 6.4% and 6.5% respectively.

Performance Analysis of Different Classifiers

In order to verify the effect of different algorithms on glaucoma fundus image classification under the same experimental environment, the performance of classical SVM, Stochastic Forest, Yuan Zhou [5], Gupta [8], Ke Shiyuan [9], DAS [10] and the algorithm in this paper were analyzed, the analysis results shown in Table 2.

Table 2. Performance analysis of different classifiers (%)

Method	Acc	Sp	Sn
SVM	89.92	87.85	89.02
Stochastic forest	89.80	86.32	88.64
YuanZhou	92.84	91.12	94.21
Gupta	90.76	83.30	96.10
Ke Shiyuan	92.24	89.13	95.50
DAS	91.47	88.82	92.15
Proposed method	94.46	91.74	95.89

It can be seen from Table 2 that the best is the algorithm studied in this paper and its accuracy, specificity and sensitivity of the improved algorithm are 94.46%, 91.74% and 95.89% respectively, which is 3.6%, 4.5% and 3.5% higher than the traditional algorithm. The improved algorithm has some advantages in fundus image detection.

Ablation Experiment

To verify that the proposed algorithm has a good effect on the detection of glaucoma lesions, a study was made on the ablation of the proposed algorithm under the same experimental environment, and the average detection results were evaluated using the accuracy rate, The results of the evaluation are shown in Table 3.

Table 3. Performance analysis of different classifiers (%)

Unet++	Butterworth filter	Power Function Method of Fusing Butterworth	Attention mechanism	Residual convolution module	Acc
					85.28
✓	✓				86.00
✓	✓		✓		86.59
✓	✓		✓	✓	87.21
✓		✓			87.88
✓		✓	✓		88.79
✓	✓	✓	✓	✓	94.46

This can be seen from Table 3, the traditional UNet++ network model is optimized by using the Butterworth power function and residual theory, which has some advantages in classifying glaucoma fundus lesions.

4   Conclusion

An improved UNet++ network model of C4.5 decision tree is proposed. The model can preprocess the green channel image, then enhance the texture of the feature image by using the improved UNet++ network. Finally, the decision tree was used to get the severity of glaucoma. The algorithm can be applied to classify and detect glaucoma fundus diseases, as well as other medical images and traffic images, but the training time and classification accuracy of the network model need to be further optimized.

References

1. Aich, G., Banerjee, G., Debnath, S., Sen, A.: Optical disc segmentation from color fundus image using contrast limited adaptive histogram equalization and morphological operations. In: 2021 International Conference on Smart Generation Computing, Communication and Networking (SMART GENCON), pp. 1–6 (2021). https://doi.org/10.1109/SMARTGENCON51891.2021.9645808
2. Li, X.: Research on image analysis and automatic disease diagnosis algorithm based on color fundus image. Beijing Institute of Technology (2017)
3. He, X., Xu, J., Chen, W.: Research on fundus blood vessel image segmentation based on improved U-Net network. J. Electron. Meas. Instr. **35**(10), 202–208 (2021). https://doi.org/10.13382/j.jemi.b2003781
4. Deari, S., Öksüz, İ., Ulukaya, S.: Importance of data augmentation and transfer learning on retinal vessel segmentation. In: 2021 29th Telecommunications Forum (TELFOR), pp. 1–4 (2021). https://doi.org/10.1109/TELFOR52709.2021.9653400
5. Yuan X, Guo H, Lu, L., Wei, L., Yu, Z.: High-resolution remote sensing image change detection algorithm based on UNet++ network and attention mechanism. J. Surv. Mapp. Sci. Technol. **38**(02), 155–159 (2021)
6. Serener, A., Serte, S.: Glaucoma classification via deep learning ensembles. In: 2021 International Conference on INnovations in Intelligent SysTems and Applications (INISTA), pp. 1–5 (2021). https://doi.org/10.1109/INISTA52262.2021.9548439
7. Guo, C., Li, W., Zhao, X., Zou, B.: Glaucoma screening method guided by semantic feature map. J. Comput. Aided Design Graph. **33**(03), 363–375 (2021)
8. Gupta, G., Kulasekaran, S., Ram, K., et al.: Local characterization of neovascularization and identification of proliferative diabetic retinopathy in retinal fundus images. Comput. Med. Imaging Graph. **55**(SC), 124–132 (2017)
9. Ke, S., Hu, M., Xu, Y.: Research on computer-aided glaucoma diagnosis algorithm based on ensemble learning. J. Beijing Univ. Chem. Technol. (Nat. Sci. Edn.) **46**(04), 86–91 (2019). https://doi.org/10.13543/j.bhxbzr.2019.04.013 https://doi.org/10.13543/j.bhxbzr.2019.04.013 https://doi.org/10.13543/j.bhxbzr.2019.04.013 https://doi.org/10.13543/j.bhxbzr.2019.04.013
10. Das, P., Nirmala, S.R., Medhi, J.P.: Diagnosis of glaucoma using CDR and NRR area in retina images. Netw. Model. Anal. Health Inform. Bio Inform. **5**(1), 1–14 (2016)
11. Venugopal, N., Mari, K., Manikandan, G., Sekar, K.R.: Phase quantized polar transformative with cellular automaton for early glaucoma detection. Ain Shams Eng. J. **12**(4), 4145 (2021)
12. Zhu, Z., Li, H., Zhao, L., Wang, H., Tan, J.: Research on image enhancement algorithm of magnetic tile surface defects based on improved homomorphic filtering and SMQT. Optoelectron. Laser **32**(08), 818–825 (2021). https://doi.org/10.16136/J.Joel.2021.08
13. Hao, M.: Research on underwater image enhancement method based on pyramid fusion. Dalian Maritime University (2020). https://doi.org/10.26989/D.CNKI.GDLHU.2020.000020
14. Wang, W., Chen, W., Wang, L., Yuan, J.: Research on a method of adjusting the contrast of fundus images. China Med. Equip. **12**, 11–13 (2006)
15. Zhou, Z., Rahman Siddiquee, M.M., Tajbakhsh, N., Liang, J.: UNet++: a nested U-net architecture for medical image segmentation. In: Stoyanov, D., et al. (eds.) DLMIA/ML-CDS -2018. LNCS, vol. 11045, pp. 3–11. Springer, Cham (2018). https://doi.org/10.1007/978-3-030-00889-5_1

16. Fu, Y., Li, Z., Zhang, Y., Pan, D.: A U-net with residual module for detecting the exudation of fundus images. Minicomput. Syst. **42**(07), 1479–1484 (2021)
17. Chen, H., Zhen, X., Zhao, T.: A small target detection model based on channel-spatial attention mechanism feature fusion [J/OL]. J. Huazhong Univ. Sci. Technol. (Nat. Sci. Edn.) 1–8 (2022). https://doi.org/10.13245/J.HUST.238491
18. Chen, X., Well, L., Zhang, Y., Xue, Q.: Post-nonlinear BSS algorithm based on multilayer neural network and PReLU function. J. Mianyang Norm. Univ. **39**(02), 25–30+46 (2020). https://doi.org/10.16276/j.cnki.cn51-1670/g.2020.02.006
19. Fang, C., Fan, M.: Text detection based on improved convolutional neural network and line features. Microelectron. Comput. **36**(08), 77–82 (2019). https://doi.org/10.19304/j.cnki.issn1000-7180.2019.08.017